

Frequency Tuning in Integrated InGaAsP/InP Ring Mode-Locked Lasers

John S. Parker, Pietro R. A. Binetti, Yung-Jr Hung, and Larry A. Coldren, *Fellow, IEEE*

Abstract—We demonstrate for the first time, continuous frequency tuning >40 MHz using symmetric phase tuning regions in an InGaAsP/InP 18 GHz passively mode-locked ring laser. Frequency tuning is achieved through current injection into passive waveguides, via the free-carrier plasma effect, which is enhanced by the concurrent increase in cavity losses from free-carrier absorption. Stable mode-locking with ~ 1 ps pulse-width is realized from -2.5 to -7.5 V bias on the saturable absorber and 170 to 290 mA drive current. The average RF power is 50 dB above the noise level over this regime.

Index Terms—Mode-locked laser, pulsed lasers, quantum well laser, ring laser, semiconductor laser.

I. INTRODUCTION

InGaAsP/InP mode-locked lasers (MLLs) operating at 1.55 μm wavelength are very stable pulsed sources, which makes them attractive components for high-speed optical fiber communication with optical-time-division-multiplexing (OTDM) [1], multi-wavelength sources for wavelength-division-multiplexing (WDM) [2], low-noise microwave oscillators [3], clock distribution systems [4], as well as for various applications in biological imaging [5]. MLLs built on a highly versatile InGaAsP/InP material platform provide the capability to create monolithically integrated systems-on-chip when combined with components that include: widely-tunable transmitters [6], balanced receivers [7], tunable optical filters [8], wavelength converters [9], and pulse-shapers [10]. New applications in microwave photonics may benefit from integrated mode-locked lasers used for high-frequency stable on-chip RF sources, such as the recently demonstrated integrated Optical Phase-Lock-Loop (OPLL) built on the InGaAsP/InP material platform [11].

Considerable work has been done in mode-locked laser cavity designs on InP including: Fabry–Perot (FP) [12], Distributed-Bragg-Reflector (DBR) [13], and ring resonator [14]. The ring

MLL has an advantage in that it can be defined entirely by photolithography without the need for electron beam lithography or holography to create DBR gratings, and it avoids repetition rate errors from cleaving, common on FP and DBR designs. Cleaving errors for conventional systems are at best $\pm 5 \mu\text{m}$, corresponding to ± 50 MHz on a 20 GHz DBR laser [15]. Such errors can be reduced by dry-etching the facets [16], however drawbacks do arise. Furthermore, the repetition rate on DBRs is determined by the effective penetration depth into the mirror sections, which is highly dependent on the grating etch depth, adding a further degree of repetition rate variation in processing.

For ring MLL, the repetition rate can be set entirely by optical lithography with better than 1 μm accuracy, i.e., 5 MHz repetition rate accuracy for a 20 GHz InGaAsP/InP MLL. Even greater precision is often necessary for optical communication and clocking applications. The drive current of the laser and the bias on the saturable absorber can be used to shift the repetition rate of the laser, however it is advantageous to fix these operating parameters at the most optimal mode-locking condition, e.g., lowest jitter, highest RF power, or narrowest pulse-width. Integrated hybrid or active mode-locking offers one solution, where by applying an RF drive signal on the saturable absorber an external microwave source determines the repetition rate. The RF drive signal must within the locking bandwidth and closely matched to a multiple of the cavity length for efficient power coupling from the RF source [15]. For this reason, tuning the cavity length to match the desired repetition rate is desirable for both hybrid and passive mode-locking.

Phase tuning pads alter the effective refractive index of the material, provide precise phase engineering of the passive ring length, and allow continuous tuning of the repetition rate. The effect is enhanced by increased cavity losses due to free-carrier absorption, which occurs from current injection in the passive sections. The phenomenon has been studied extensively to achieve frequency tuning in DBR MLL [15], [17], [18], and tuning as much as 400 MHz at a 40 GHz repetition rate has been demonstrated [17]. To our knowledge this is the first integrated ring MLL with phase pads, which has the advantage of avoiding gratings allowing for easier, less expensive processing, and the capability to determine the repetition rate entirely by lithography.

II. FABRICATION

A standard offset quantum well (QW) InGaAsP/InP integrated platform is used with 7 QWs positioned above a 300 nm tall 1.3 Q waveguide with a modal confinement factor of 7.1% [19]. A wet-etch removes the QWs for low loss passive waveguides followed by a single blanket 1.8 μm p+ InP cladding

Manuscript received October 27, 2011; revised January 07, 2012; accepted January 11, 2012. Date of publication January 13, 2012; date of current version April 04, 2012. This work was supported by the Defense Advanced Research Project Agency (DARPA) Photonic Integrated for Coherent Optics (PICO) program. A portion of this work was done in the UCSB nanofabrication facility, part of the National Science Foundation (NSF)-funded NNIN network.

J. S. Parker, P. R. A. Binetti, and L. A. Coldren are with the Department of Electrical and Computer Engineering, University of California, Santa Barbara, CA 93106 USA (e-mail: JParker@ece.uscb.edu).

Y.-J. Hung is with the Department of Electronic Engineering, National Taiwan University of Science and Technology, Taipei 106, Taiwan.

Color versions of one or more of the figures in this paper are available online at <http://ieeexplore.ieee.org>.

Digital Object Identifier 10.1109/JLT.2012.2184264

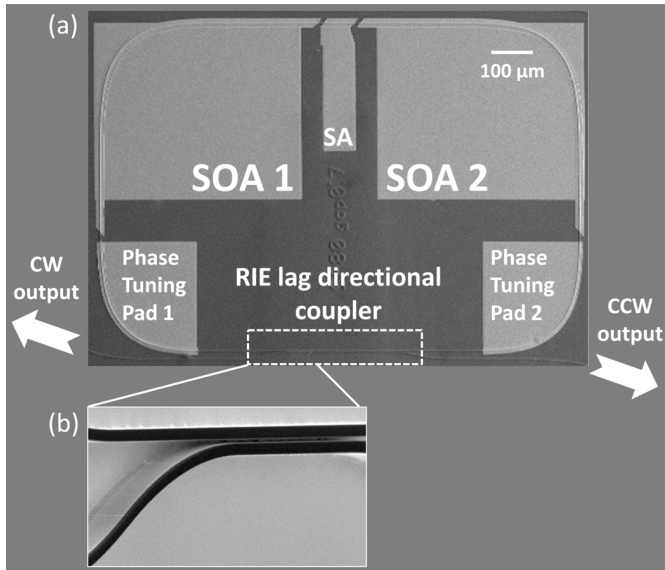


Fig. 1. (a) Scanning electron microscope (SEM) image of fabricated ring mode-locked laser with semiconductor optical amplifiers (SOAs), saturable absorber (SA), phase tuning pads, and directional coupler. (b) SEM side-view of two waveguides coming together to form the directional coupler.

regrowth, a 150 nm p++ InGaAs contact layer, and a 400 nm p+ InP protective cap. Waveguides are defined by stepper lithography on a photoresist/Cr/SiO₂ three-layer mask. The Cr is etched using a Cl₂/O₂ (23.3/6.8 sccm) inductively coupled plasma (ICP) reactive-ion etch (RIE) with 50 W ICP and 15 W bias power at 10 mT chamber pressure. The SiO₂ mask is etched with a SF₆/Ar (50/10 sccm) based ICP RIE using 600 W ICP and 50 W bias power at 7.5 mT. The SiO₂ is used to mask the InGaAsP/InP in Cl₂/H₂/Ar (9/18/2 sccm) ICP RIE with 850 W ICP power and 125 W bias power at 1.5 mT.

The RIE lag effect [20], which acts to slow the etch rate of smaller features, is used to define a 300 μm long directional coupler on a deeply etched 4400 μm ring with a single etch-step as shown in Fig. 1. Each of the two phase tuning pads are 500 μm long, the saturable absorber (SA) is 80 μm, and the two semiconductor optical amplifiers (SOAs) are 1200 μm. The remainder of the ring is passive waveguide. The waveguide width is 1.8 μm.

The directional coupler is chosen to minimize unwanted back-reflections in the ring structure, which would perturb stable MLL operation. The directional coupler has an etch depth of ~2.5 μm (150 nm etch into the waveguide layer at the center, and 175 nm etch into the waveguide layer at the edge), whereas the etch depth of the deeply etched waveguides is 3.61 μm (below the waveguide layer by 960 nm), as shown in Fig. 2. A deeply etched directional coupler needs an extremely narrow gap <300 nm to have appreciable coupling. This typically requires more complicated Electron-Beam-Lithography (EBL), while the severe RIE lag effect, due to reduced etch rates in high aspect-ratio features, necessitates long etch times. This high aspect-ratio etch is difficult to make vertical and smooth, which increases scattering losses.

We overcome these issues by adopting the single-etch process, which uses the RIE lag to our advantage and allows more streamlined processing of directional couplers

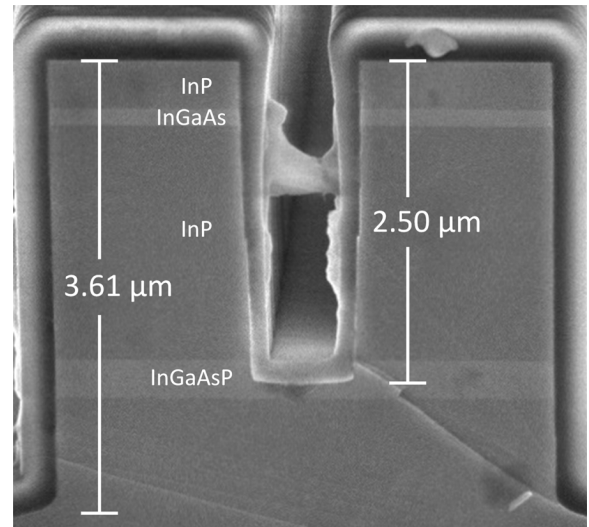


Fig. 2. SEM cross section of RIE lag directional coupler. The center etch depth is 150 nm into the waveguide layer. The outer etch depth is 960 nm below the waveguide layer.

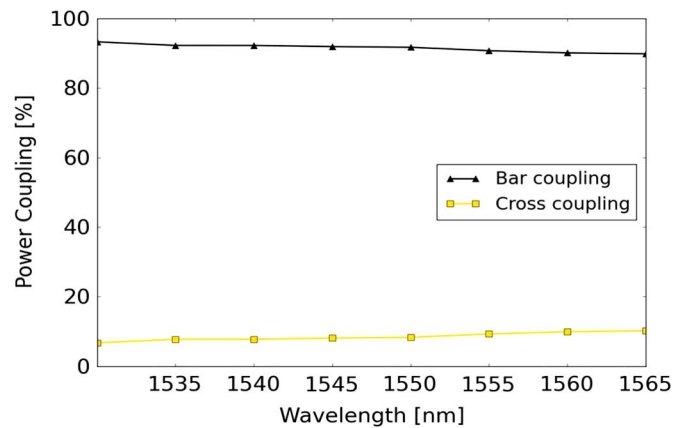


Fig. 3. Measured wavelength dependence of RIE lag directional coupler.

without the need for a separate surface ridge waveguide defined by wet-etching and deeply etched waveguide defined by dry-etching. The etch depth is controlled by timing the etch rate and measuring SEM cross-sections on a test sample. The 700 nm wide 300 μm long directional coupler has cross coupling of ~10% at 1550 nm, as shown in Fig. 3. This is measured by fiber coupling a tunable laser into the access waveguide of the directional coupler. To act as on-chip photodetectors, two 300 μm SOAs are placed symmetrically on the coupler output ports and reverse biased at -3 V. These couplers measure the incident optical power as the tunable laser is swept from 1530 to 1565 nm.

The directional coupler is simulated using RSoft BeamProp software as shown in Fig. 4. The results match well; the measured data falls between the simulated 125 and 150 nm etch depth curves. The simulation provides further insight into the tolerance of the device with etch depth, as shown in Fig. 5. For a fixed length, the cross-coupling is highly dependent on the etch depth and 300 μm length couplers can be fabricated with 1% to 80% power coupling. Fabrication tolerance is increased

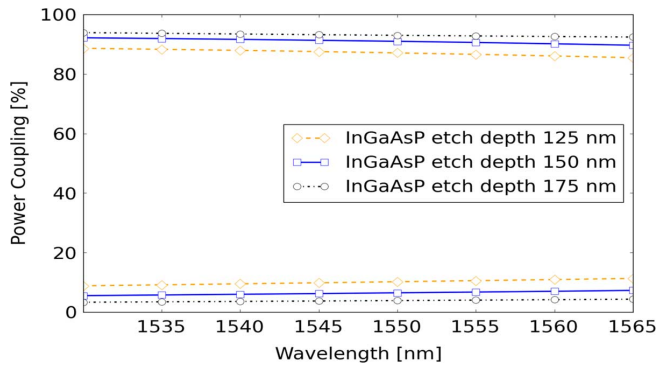


Fig. 4. Simulated wavelength dependence of RIE lag directional coupler.

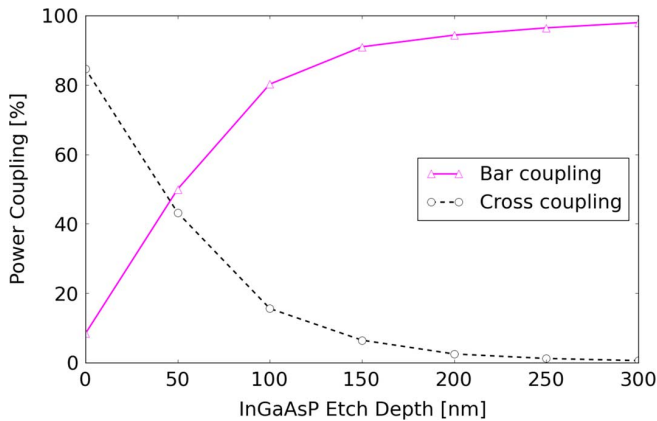


Fig. 5. Simulated etch depth dependence of RIE lag directional coupler.

by designing the lag coupler for deeper etch depths, where the slope of the coupling function changes more slowly.

After waveguide definition, the ridges are covered with 350 nm of SiN_x and vias are opened for P-type Pt/Ti/Pt/Au contacts. The backside substrate of the semiconductor is lapped to 110 μm thickness and N-type Ti/Pt/Au contacts are deposited. The P-type contacts are electrically isolated from each other using a proton implant, which provides 20 k Ω resistance between contacts spaced 10 μm apart.

III. MODE-LOCKING

Mode-locked lasers are soldered to copper blocks, placed on a thermo-electric cooler, and tested at 15°C. Mode-locking is typically defined as a peak RF power 25 dB above the noise floor. For our measurements, we add the criterion that the RF peak power must also be 25 dB above any side-peaks or undesirable frequency spurs.

We measure lasing threshold at 80 mA and peak mode-locked lasing power of 1.2 mW in each direction from on-chip reverse biased SOA detectors; the on-chip detectors are biased at transparency for off-chip testing. Based on the 10% coupler, we calculate the average lasing power inside the ring to be ~ 12 mW. The device has long access waveguides ~ 1500 μm ending in 7° flared waveguides with AR coatings to minimize back reflections. Lensed fiber is used to capture the output power with a measured coupling loss of 5 dB. The measured peak power off-chip is 200 μW (-7 dBm).

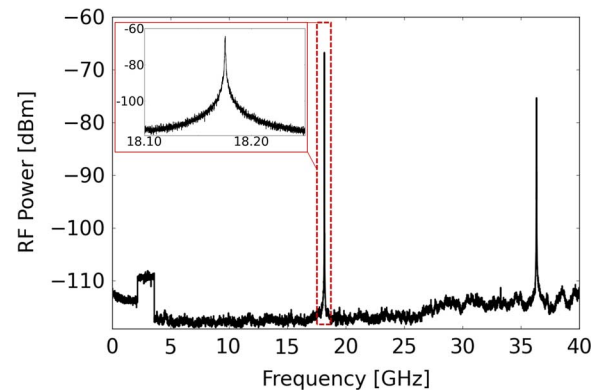


Fig. 6. Measured RF-spectrum $I_{\text{SOA}} = 210$ mA, $V_{\text{SA}} = -4.5$ V. The step discontinuity at 3 GHz is due to electronic amplifier.

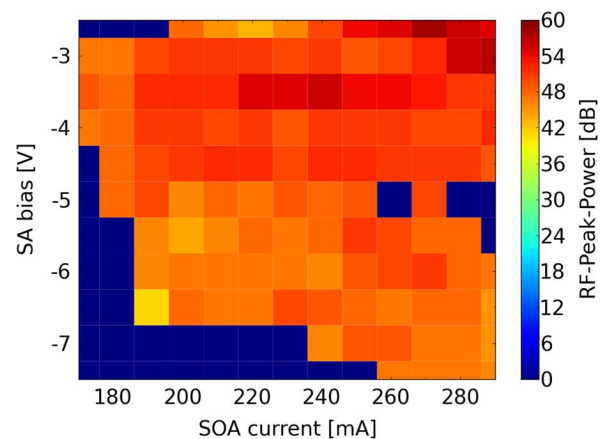


Fig. 7. RF peak power over the operating region. Average RF power is 50 dB above the noise. The blue regions of the color map are regions that did not meet the criterion for mode-locking.

SA and SOA settings are swept to map out the stable mode-locking regime. The sweeps are restricted to -2.5 to -7.5 V SA bias and 170–290 mA SOA drive current to focus on the central region of operation, in which more than 90% of the mode-locking regime occurs. The RF spectra of the fundamental and second harmonic from the ring MLL is shown in Fig. 6 from measurements on a Rohde Schwarz 50 GHz electrical spectrum analyzer (ESA) with a U² T 50 GHz photodiode. A 30 dB low noise amplifier is used to boost the RF signal, as the input power into the photodiode is quite low.

The raised plateau on the RF spectra at 3 GHz is due to distortion from the low noise amplifier and appears regardless of input signal. The RF peak power over the operating regime is shown in Fig. 7, and the -20 dB linewidth of the RF power in Fig. 8. The average -20 dB linewidth is 5.9 MHz, the minimum -20 dB linewidth is 1.5 MHz, and the average RF power is 50 dB.

The pulse-width variation is measured by an Inrad SHG autocorrelator (AC) and is shown in Fig. 9. Before the AC, the pulse-train is sent through a 30 dBm EDFA to provide enough optical power for clear autocorrelation traces. The signal-to-noise ratio (SNR) of these autocorrelation traces is as high as 13 dB, and most operating points are near this SNR; at the edges of the operating regime, the SNR decreases rapidly. The pulse-width map

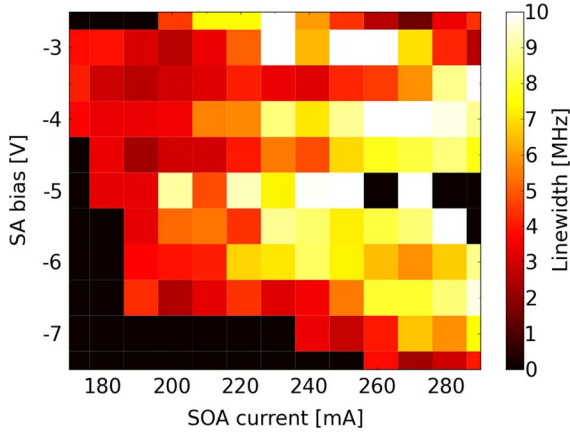


Fig. 8. RF -20 dB linewidth over the operating region. Average -20 dB linewidth is 5.9 MHz. The black regions of the color map are regions that did not meet the criterion for mode-locking. The white regions are mode-locked with a linewidth > 10 MHz.

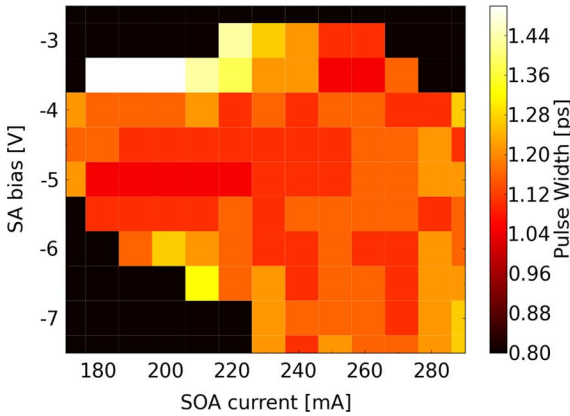


Fig. 9. Gaussian pulsewidth over the operating region. The black regions of the color map are regions that did not meet the criterion for mode-locking. The white regions are mode-locked with a pulse-width > 1.5 ps.

is limited to autocorrelation traces with $\text{SNR} > 6$ dB, such that the amplitude at full-width-half-maximum (FWHM) is at least twice the noise level. At 3 dB SNR, the FWHM is obscured by the noise level; at 6 dB, the FWHM is significantly above the noise floor and allows clear measurements of the pulse-width. The cross-correlation is also measured to ensure that the pulses are indeed mode-locked.

For consistency, the pulse-widths are all measured assuming a Gaussian pulse shape. The Gaussian shape results in the widest FWHM after deconvolving the autocorrelation. However, the measured pulse shape does change over the operating regime and the Gaussian shape is not always the most accurate in fitting. In this case, the Gaussian shape provides a conservative upper limit on pulse-width (Lorentzian or hyperbolic secant fitting results in a narrower pulse-width). For example, the fit for a measured 1.1 ps Gaussian pulse is shown in Fig. 10, the hyperbolic secant has an $R^2 = 0.95$, whereas the Gaussian has an $R^2 = 0.90$.

The optical spectrum of the mode-locked laser is measured on the optical spectrum analyzer (OSA), as shown in Fig. 11 at -5 V reverse bias and 220 mA drive current, corresponding to a 1 ps pulse-width. The FWHM of the optical spectrum is 5.3 nm,

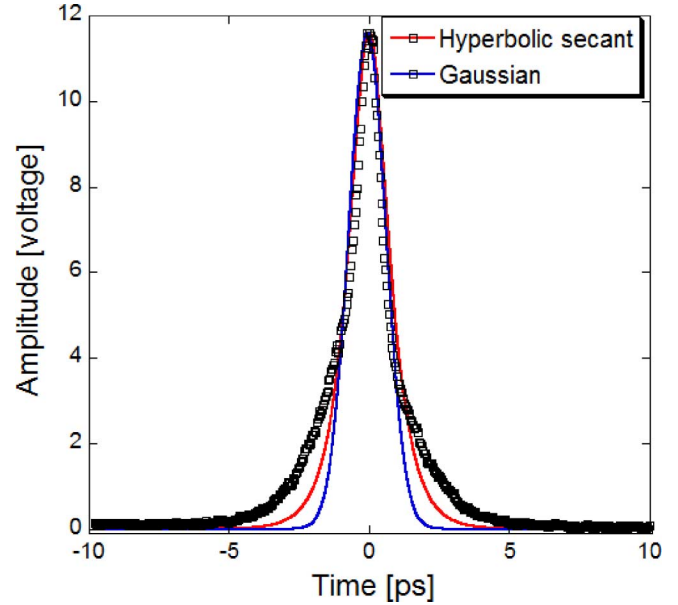


Fig. 10. Measured autocorrelation trace with hyperbolic secant and Gaussian curve fits, with R^2 values of 0.95 and 0.90, respectively. The operating conditions are 180 mA SOA current and -4 V reverse bias on the absorber.

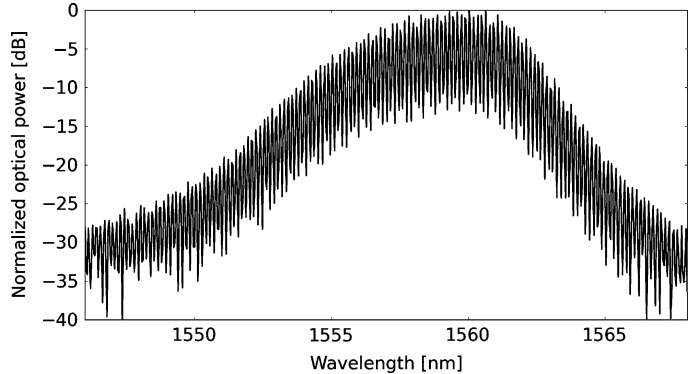


Fig. 11. Measured optical spectrum at 220 mA drive current and 5 V reverse bias on the saturable absorber. FWHM is 5.3 nm.

and the resulting time-bandwidth product is 0.66. The Gaussian time-bandwidth limit is 0.44. Hence, the output pulses from the MLL likely have a frequency chirp that is responsible for this deviation from the time-bandwidth limit.

There are some operating points that differ on the RF peak power and the pulse-width map, these measurements do not fit the criterion for RF tones > 25 dB above side-spurs (on the RF map), and for autocorrelation traces with $\text{SNR} > 6$ dB. These operating points might be acceptable for some applications, however this mode-locking is not ideal.

IV. FREQUENCY TUNING

Two $500 \mu\text{m}$ passive waveguide sections allow continuous frequency tuning of the fundamental mode-locked tone. By injecting carriers into the P-i-N junction in these regions, the carrier density is increased and the effective index of refraction of the material is decreased, due the free-carrier plasma effect. A lower effective index decreases the round-trip cavity flight-time and increases the repetition frequency. The total phase pad

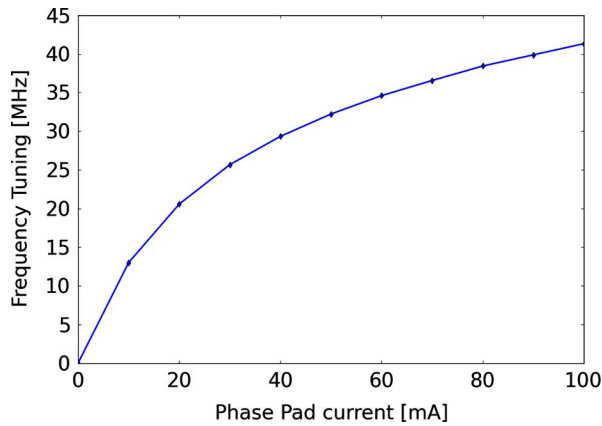


Fig. 12. Frequency tuning of the ring MLL by injecting current into both phase pads. The total phase pad length is $1000 \mu\text{m}$. Stable mode-locking is observed over the entire range of phase pad currents.

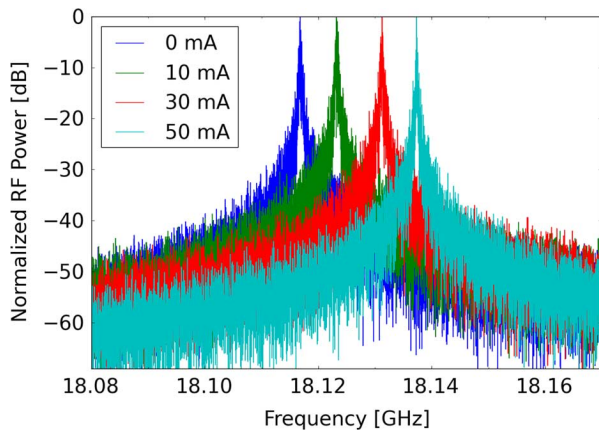


Fig. 13. RF spectra as the phase pad current in one pad is increased from 0 to 50 mA, and the frequency is tuned by ~ 20 MHz. Stable mode-locking occurs over the entire range of tuning currents.

length is $1000 \mu\text{m}$ or 22% of the total ring length. The frequency tuning is measured on the ESA for an SA bias of -4 V and an SOA drive current of 220 mA, as shown in Fig. 12. Mode-locking is maintained over the entire range of phase pad currents. The frequency shift of the RF spectra from a single phase pad is shown in Fig. 13.

The phase pads provide repetition rate frequency tuning of 41 MHz, for this $4400 \mu\text{m}$ cavity. To measure the refractive index shift of the phase pads, the ring is operated below lasing and the resonator comb shift is measured on an optical spectrum analyzer (OSA) with 0.06 nm resolution. From the OSA, phase tuning of $\sim 8\pi$ is measured, i.e., a change in the effective cavity length by $1.63 \mu\text{m}$ and an index shift in the phase pad sections of $5.3e-3$ (0.16%). Such an index shift, results in a change in the round-trip flight time by 0.037%. However, the repetition rate frequency tunes by 0.22%, due to an enhancement from the added loss of the phase pad as described in [17], [18]. This is a $\sim 6X$ enhancement factor ($0.22\%/0.037\%$) in repetition rate tuning due to the phase pad loss.

With the phase pads open, i.e., with a floating voltage, the propagation loss is 28 dB/cm. An intracavity method is used

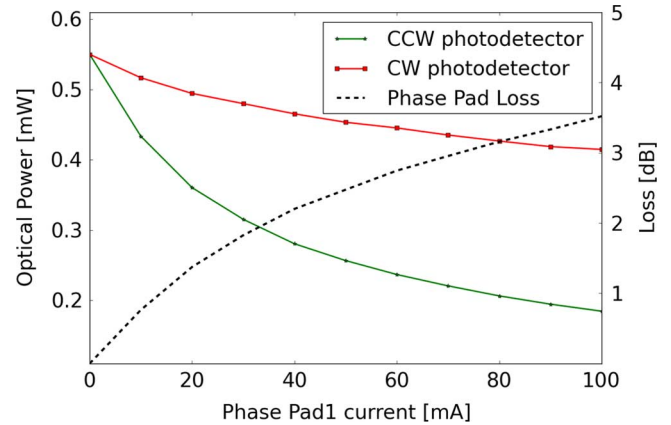


Fig. 14. Continuous-wave (not mode-locked) directional power tuning by asymmetrically biasing the phase pads. The plot shows output power in the clockwise (CW) and counter-clockwise (CCW) direction as a single phase pad is biased. The power is measured by on-chip photodetectors (not shown in Fig. 1).

to measure the added loss from tuning a single phase pad. In this measurement the SA in the MLL is forward biased at 2 V (i.e., the laser is free-running and not mode-locked) and the SOAs are driven at 120 mA to keep the ring just above lasing, thus preventing unidirectional operation as occurs under continuous-wave operation at high photon densities [21]. As shown in Fig. 14, at 0.55 mW output power both CW and CCW ports decrease as current to Phase Pad1 is increased. The phase pad loss is found from the difference between the two output directions. A phase change of π occurs at 3.5 mA phase pad current with an insertion loss of 0.6 dB.

This difference in output power shown in Fig. 14 is expected, and is well predicted by simple cavity geometry. Consider current applied to Phase Pad1, the CCW direction has the loss element before the output coupler, whereas the CW direction has the loss element after the output. In this case, both lasing directions have an equal increase in threshold gain due to the phase pad loss. However, the difference in output power between the two directions is entirely due to the single pass loss of the phase pad.

The common method to calculate the phase pad loss involves fiber coupling an off-chip laser into the structure, and using the ring SOAs in reverse bias as detectors to measure the change in optical transmission. Our measurements using this common method are in agreement, ~ 3 dB at 100 mA phase pad current, however fluctuations in coupled optical power due to vibrations and drift in the mechanical positioner are avoided using the intracavity method, reducing the uncertainty of the measurement.

A phase pad provides a tunable low-loss element inside the cavity, which can also be used to investigate the effects of carrier density in future mode-locking experiments. For lasers operating above lasing threshold, the carrier density clamps and is independent of drive current. Therefore, without changing the temperature, most lasers can only operate at a single specific current density. Since the phase pads add loss to the cavity, they can be used to precisely adjust the threshold gain and carrier density during lasing.

V. CONCLUSION

We have demonstrated the first integrated ring mode-locked laser with phase pads. The phase pads provide continuous frequency tuning of the repetition rate by >40 MHz. Ring mode-locked lasers with precise frequency tuning have applications in clocking and WDM data communication with tightly defined spacing for the frequency grid. We have presented a novel method using a ring laser to characterize the loss of the phase pads with high precision.

REFERENCES

- [1] V. Kaman and J. E. Bowers, "120 Gbit/s OTDM system using electroabsorption transmitter and demultiplexer operating at 30 GHz," *Electron. Lett.*, vol. 36, no. 17, pp. 1477–1479, 2000.
- [2] Y. B. M'Sallem, Q. T. Le, L. Bramerie, Q. Nguyen, E. Borgne, P. Besnard, A. Shen, F. Lelarge, S. LaRochelle, L. A. Rusch, and J. Simon, "Quantum-dash mode-locked laser as a source for 56-Gb/s DQPSK modulation in WDM multicast applications," *IEEE Photon. Technol. Lett.*, vol. 23, no. 7, pp. 453–455, Apr. 2011.
- [3] T. M. Ramond, A. Bartels, S. A. Diddams, L. Hollberg, and H. Kurz, "Low instability, low phase-noise femto-second optical frequency comb microwave synthesizer," in *Proc. IEEE Int. Freq. Control Symp. PDA Exhib. 17th Europ. Freq. Time Forum*, Tampa, FL, May 2003, pp. 168–171.
- [4] P. J. Delfyett, D. H. Hartman, and S. Z. Ahmad, "Optical clock distribution using a mode-locked semiconductor laser diode system," *J. Lightw. Technol.*, vol. 9, no. 12, pp. 1646–1649, Dec. 1991.
- [5] W. Drexler, "Ultrahigh-resolution optical coherence tomography," *J. Biomed. Opt.*, vol. 9, no. 1, pp. 47–74, 2004.
- [6] J. S. Barton, E. J. Skogen, M. L. Masanovic, S. P. Denbaars, and L. A. Coldren, "A widely tunable high-speed transmitter using an integrated SGDBR laser-semiconductor optical amplifier and Mach-Zehnder modulator," *IEEE J. Sel. Topics Quantum Electron.*, vol. 9, no. 5, pp. 1113–1117, Sep.-Oct. 2003.
- [7] J. Klamkin, A. Ramaswamy, L. A. Johansson, H.-F. Chou, M. N. Sysak, J. W. Raring, N. Parthasarathy, S. P. DenBaars, J. E. Bowers, and L. A. Coldren, "High output saturation and high-linearity uni-traveling-carrier waveguide photodiodes," *IEEE Photon. Technol. Lett.*, vol. 19, no. 3, pp. 149–151, Feb. 2007.
- [8] E. J. Norberg, R. S. Guzzon, S. C. Nicholes, J. S. Parker, and L. A. Coldren, "Programmable photonic lattice filters in InGaAsP/InP," *IEEE Photon. Technol. Lett.*, vol. 22, no. 2, pp. 109–111, Jan. 2010.
- [9] M. M. Dummer, M. N. Sysak, A. Tauke-Pedretti, J. W. Raring, J. Klamkin, and L. A. Coldren, "Widely tunable separate absorption and modulation wavelength converter with integrated microwave termination," *J. Lightw. Technol.*, vol. 26, no. 8, pp. 938–944, Aug. 2008.
- [10] M. J. R. Heck, P. Munoz, B. W. Tilma, E. A. J. M. Bente, Y. Barbarin, O. Yok-Siang, R. Notzel, and M. K. Smit, "Design, fabrication and characterization of an InP-based tunable integrated optical pulse shaper," *IEEE J. Quantum Electron.*, vol. 44, no. 4, pp. 370–377, Apr. 2008.
- [11] S. Ristic, A. Bhardwaj, M. J. Rodwell, L. A. Coldren, and L. A. Johansson, "An optical phase-locked loop photonic integrated circuit," *J. Lightw. Technol.*, vol. 28, no. 4, pp. 526–538, Feb. 2010.
- [12] M. J. R. Heck, A. Renault, E. A. J. M. Bente, O. Yok-Siang, M. K. Smit, K. S. E. Eikema, W. Ubachs, S. Anantathanasarn, and R. Notzel, "Passively mode-locked 4.6 and 10.5 GHz quantum dot laser diodes around 1.55 μm with large operating regime," *IEEE Sel. Topics Quantum Electron.*, vol. 15, no. 3, pp. 634–643, May–Jun. 2009.
- [13] I. Ogura, H. Kurita, T. Sasaki, and H. Yokoyama, "Precise operation-frequency control of monolithic mode-locked laser diodes for high-speed optical communication and all-optical signal processing," *Opt. Quantum Electron.*, vol. 33, pp. 709–725, 2001.
- [14] Y. Barbarin, E. A. J. M. Bente, M. J. R. Heck, Y. S. Oei, R. Nötzel, and M. K. Smit, "Characterization of a 15 GHz integrated bulk InGaAsP passive modelocked ring laser at 1.53 μm ," *Opt. Exp.*, vol. 14, no. 21, pp. 9716–9727, 2006.
- [15] R. Kaiser and B. Huttel, "Monolithic 40-GHz mode-locked MQW DBR lasers for high-speed optical communication systems," *IEEE J. Sel. Topics Quantum Electron.*, vol. 13, no. 1, pp. 125–135, Jan.–Feb. 2007.
- [16] J. S. Parker, E. J. Norberg, R. S. Guzzon, S. C. Nicholes, and L. A. Coldren, "High verticality InP/InGaAsP etching in Cl₂/H₂/Ar inductively coupled plasma for photonic integrated circuits," *J. Vac. Sci. Technol. B*, vol. 29, pp. 011016–011020, 2011.
- [17] H. F. Liu, S. A. Arahira, T. Kunii, and Y. Ogawa, "Tuning characteristics of monolithic passively mode-locked distributed Bragg reflector semiconductor lasers," *IEEE J. Quantum Electron.*, vol. 32, no. 11, pp. 1965–1975, Nov. 1996.
- [18] S. Arahira and Y. Ogawa, "Repetition-frequency tuning of monolithic passively mode-locked semiconductor lasers with integrated extended cavities," *IEEE J. Quantum Electron.*, vol. 33, no. 2, pp. 255–264, Feb. 1997.
- [19] L. A. Coldren, S. C. Nicholes, L. Johansson, S. Ristic, R. S. Guzzon, E. J. Norberg, and U. Krishnamachari, "High performance InP-based photonic ICs—A tutorial," *J. Lightw. Technol.*, vol. 29, no. 4, pp. 554–570, Feb. 2011.
- [20] Y. Shi, S. He, and S. Anand, "Ultracompact directional coupler realized in InP by utilizing feature size dependent etching," *Opt. Lett.*, vol. 33, no. 17, pp. 1927–1929, 2008.
- [21] M. Sorel, P. J. R. Laybourn, G. Giuliani, and S. Donati, "Unidirectional bistability in semiconductor waveguide ring lasers," *Appl. Phys. Lett.*, vol. 80, pp. 3051–3053, 2002.